

©2018. American Geophysical Union. All Rights Reserved

Access to this work was provided by the University of Maryland, Baltimore County (UMBC) ScholarWorks@UMBC digital repository on the Maryland Shared Open Access (MD-SOAR) platform.

**Please provide feedback**

Please support the ScholarWorks@UMBC repository by emailing [scholarworks-group@umbc.edu](mailto:scholarworks-group@umbc.edu) and telling us what having access to this work means to you and why it's important to you. Thank you.

## Diurnal variation of 340 nm Lambertian equivalent reflectivity due to clouds and aerosols over land and oceans

Gordon J. Labow,<sup>1</sup> Jay R. Herman,<sup>2</sup> Liang-Kang Huang,<sup>1</sup> Steven A. Lloyd,<sup>3</sup> Matthew T. DeLand,<sup>1</sup> Wenhan Qin,<sup>1</sup> Jianping Mao,<sup>4</sup> and David E. Larko<sup>1</sup>

Received 30 August 2010; revised 2 March 2011; accepted 9 March 2011; published 8 June 2011.

[1] Thirty years of satellite measurements of Lambert equivalent reflectivity (LER) at 340 nm have been analyzed to show the changes in diurnal LER that are associated with cloud and aerosol amounts. Five degree zonal mean diurnal variations of LER are obtained from multiple NASA and NOAA satellites making 340 nm LER measurements from 0600 to 1800 local solar time. These zonal means were calculated separately over water and land. The results show different behavior of clouds over oceans with LER peaking in the morning compared to LER over land, which peaks in the afternoon. Over the oceans the cloud amount increases as a function of latitude in both hemispheres, with the exception of the midtropics (10–20°). Over land, the amount of cloudiness significantly decreases by almost a factor of 2 from the equator to ~25° and then, in the Northern Hemisphere, increases as a function of latitude. The zonal means represent measured cloud amounts, and thus a quantification of energy reflected back into space as a function of time of day. Cloud fraction measurements made by Aqua and Terra Moderate Resolution Imaging Spectroradiometer show a signature that is similar to the measured ratios of LER in morning to afternoon. The similarity in pattern demonstrates that the LER is measuring a quantity directly related to cloud fraction.

**Citation:** Labow, G. J., J. R. Herman, L.-K. Huang, S. A. Lloyd, M. T. DeLand, W. Qin, J. Mao, and D. E. Larko (2011), Diurnal variation of 340 nm Lambertian equivalent reflectivity due to clouds and aerosols over land and oceans, *J. Geophys. Res.*, 116, D11202, doi:10.1029/2010JD014980.

### 1. Introduction

[2] Satellite measurements of radiances at the top of the Earth's atmosphere (TOA) contain information about clouds, aerosols, absorbing gases, and the Earth's surface. In the near-UV (NUV) wavelength range ( $300 < \lambda < 400$  nm), most of the radiation coming back to the top of the atmosphere originates from Rayleigh scattering and from Mie scattering when clouds and aerosols are present. Less than 10% originates from the Earth's surface [Herman and Celarier, 1997]. For Rayleigh scattering the fraction of direct sunlight scattered back to the TOA is a strong function of wavelength  $\lambda$ , approximately proportional to  $\lambda^{-4}$ . If aerosols are present, the aerosol scattered component is approximately proportional to  $\lambda^{-1}$ , while for clouds, the diffuse reflectivity and transmission of the clouds is approximately independent of wavelength.

[3] When the satellite's field of view (FOV) is large (e.g., greater than  $50 \times 50$  km<sup>2</sup>), each FOV usually contains a mixture of clear and cloudy scenes, a mixture of different surfaces, cloud types, and scattering aerosols. The contribution to the LER value from the aerosols and the clouds cannot be separated. The radiance at the TOA can be calculated from a formal solution of the vector radiative transfer equation containing a single free parameter, the Lambert equivalent reflectivity (LER) [Chandrasekhar, 1960; Dave, 1964; Dave and Furukawa, 1964; Herman et al., 2009; Herman, 2010]. The value of the LER is obtained by requiring the calculated and measured TOA radiances to be equal (see Appendix A). The calculated LER represents the average reflectivity of an entire scene after removal of multiple Rayleigh scattering effects, and assumes that all reflecting surfaces behave as an ideal Lambertian reflector. The values of LER range from 0 to 1, but are frequently expressed as a percentage from 0 to 100. In order to avoid confusion with percent change, the LER is expressed in reflectivity units (RU), which also range from 0 to 100.

[4] The LER study described in this paper uses a common 340 nm wavelength channel with a band pass of 1.1 nm full width at half maximum (FWHM) from the TOMS, SBUV/2, and OMI series of satellites (Total Ozone Mapping Spectrometer, solar backscatter ultraviolet (/2), and Ozone Monitoring Instrument). This wavelength was chosen because it

<sup>1</sup>Science Systems and Applications, Inc., Lanham, Maryland, USA.

<sup>2</sup>Joint Center for Earth Systems Technology Center, University of Maryland Baltimore County, Catonsville, Maryland, USA.

<sup>3</sup>Wyle Information Services, McLean, Virginia, USA.

<sup>4</sup>Goddard Earth Sciences and Technology Center, University of Maryland Baltimore County, Catonsville, Maryland, USA.

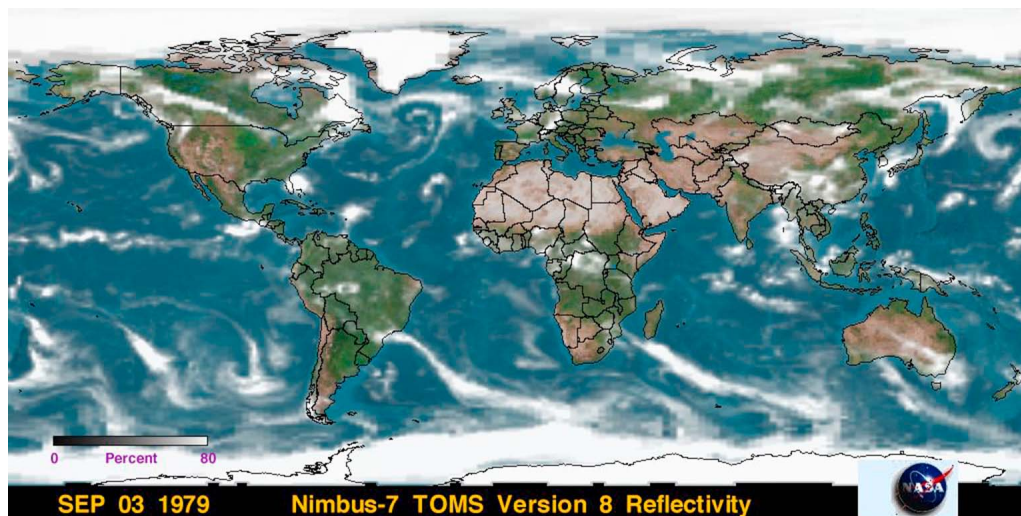


**Figure 1.** Near-UV (NUV) Lambert equivalent reflectivity (LER) (white and gray) as observed near local noon by Nimbus 7 Total Ozone Mapping Spectrometer (TOMS) on 3 September 1979, superimposed on a Moderate Resolution Imaging Spectroradiometer (MODIS) visible color map.

is the only common wavelength between the satellites, and the correction for absorption by atmospheric ozone is small. Satellite scenes at 340 nm LER include highly reflective clouds (up to  $\sim 80$  RU) which vary in time and space over a background of dark land or ocean surfaces (3 to 10 RU) [Herman and Celarier, 1997]. The highest reflectivity scenes (98 RU) contain cloud-free skies over thick, fresh snow cover, and lowest reflectivity scenes (3 RU) are found over cloud-free portions of the South Pacific Ocean. LER measurements derived from radiances reflected back to space combine the effect of cloud fraction, cloud optical depth, and aerosol optical depth from all types of cloud plus aerosol cover. Small sulfate aerosol particles scatter UV radiation with little or no absorption, and are indistinguishable from thin clouds in the LER. Dust plumes (e.g., Saharan and Gobi desert dust storms) both scatter and absorb in the NUV as can other absorbing aerosol particles (e.g., black carbon, industrial smog and biomass burning) occur annually in localized regions. The LER retrieval cannot separate cloud from aerosol contributions using a single wavelength retrieval, nor can it distinguish between different cloud types. LER is a quantitative measure of the total amount of light (energy) reflected back from the planet into space throughout the day.

[5] For a satellite in a low-Earth polar orbit (LEO), which repeatedly crosses the equator at roughly the same local solar time each day, the time series of LER represents secular changes in cloud, aerosol, and surface reflectivity. A series of LER measurements from satellites at different equator-crossing times, as well as from several LEO satellites that slowly precess over a period of years, provide a measure of the diurnal variability of LER. Diurnal variability arises from changes in cloud plus aerosol amount and geometric changes caused by the changing solar zenith angle with respect to the three dimensional distribution of cloud fields (geometrical cloud thickness, number of clouds per  $\text{km}^2$ , and multilayer clouds). The small seasonal and long-term changes in the low-NUV reflectivity of the Earth's surface (e.g., excluding snow or ice covered surfaces) do not signifi-

cantly contribute to the diurnal variability of the LER since the diurnal variability of the surface is, at most, a few RU.

[6] During the past 32 years (1979 to 2010) a series of satellites have been continuously measuring NUV radiances at the TOA and reporting the LER as a secondary data product. These are the NASA Total Ozone Monitoring satellite instruments (Nimbus 7 TOMS, Meteor 3 TOMS, ADEOS TOMS and EarthProbe TOMS), the NOAA solar backscatter ultraviolet (/2) instruments (Nimbus 7 SBUV, NOAA 9 SBUV/2, NOAA 11 SBUV/2, NOAA 14 SBUV/2, NOAA 16 SBUV/2, NOAA 17 SBUV/2, NOAA 18 SBUV/2 and NOAA 19 SBUV/2), the joint U.S./Dutch Ozone Monitoring Instrument (OMI on the NASA Aura satellite), as well as on several European ozone observing instruments (GOME and GOME 2 [Koelemeijer et al., 2003; Boersma et al., 2004]). LER data sets calculated with a common retrieval algorithm (TOMS version 8) from multiple satellites have been combined with a common calibration and data quality screening as part of the NASA-MEASURES program (Making Earth System data records for Use in Research Environments). The combined LER data product provides a composite long-term, continuous data set of near-global 340 nm LER observations for the period 1979–present for use in studies where a measure of radiation reflected back to space is important (e.g., climate change and radiation budget studies) [Labow et al., 2009; Lloyd, 2005; Kelly et al., 2006; Lloyd, 2006a; Lloyd, 2006b; Lloyd and DeLand, 2006; Qin et al., 2009]. LER has previously been used for cloud trend studies using radiance data from Nimbus 7 TOMS (1979–1992) [Herman, 2010] as well as the Sea-viewing Wide Field-of-view Sensor (SeaWiFS, 1997–2008) [Herman et al., 2009]. A brief description of the 30 year composite reflectivity data set, obtained by averaging overlapping data, is given by Herman et al. [2009]. However, the cited works have not taken into account the diurnal change in cloud cover. An example of the LER cloud observations from Nimbus 7/TOMS for 3 September 1979 is given in Figure 1. The daily TOMS data show a changing cloud cover with clearly repeating seasonal patterns that are

similar to the patterns observed from geostationary weather satellite observations.

[7] The NUV observing series of satellites have different equator crossing times, some that are nearly constant over many years, and some that have slowly drifting orbits. The combined LER time series exhibits a reproducible diurnal pattern as a function of latitude that is different over oceans and land. This paper will discuss the diurnal behavior of the measured NUV LER and compare the results with cloud fraction data obtained from the two polar orbiting MODIS satellites that have nearly constant morning and afternoon equator crossing times. The present study is limited to  $\pm 60^\circ$  latitude, which excludes the ice-covered Polar Regions where it is dark throughout the day during the winter.

## 2. Satellite Observations

[8] Geostationary weather satellites show that the amount of cloud cover (cloud fraction) can change significantly throughout the day at any geographic location, but with statistically repeatable patterns between early morning, noon, and late afternoon, depending on whether the clouds are over land or water. Previous studies using infrared satellite cloud observations show significant diurnal changes in cloud fraction over land that correlate with solar heating [e.g., Bergman and Salby, 1996; Chen and Houze, 1997; Cairns, 1995], with the highest values occurring near local noon away from coastal areas. Over oceans, the cloud fraction maxima were found in the morning, corresponding to low-altitude clouds and fogs that dissipate with increased solar heating. Wylie and Woolf [2002] found that diurnal cycles of high-altitude clouds tend to have maximum amounts in the late afternoon, implying that their mechanism of formation is different than for the lower-altitude clouds. Some coastal areas experience cloud increases in the afternoon (e.g., Florida) that are associated with convective activity and thunderstorms, while others experience morning fog and haze (e.g., the California coast). Ocean areas frequently have maximum cloud cover during morning hours from low-altitude marine stratus clouds that evaporate during the day because of warming induced by cumulative solar irradiance [Wylie, 2008].

[9] Diurnal changes in cloud cover are frequently studied at IR wavelengths from polar orbiting and geostationary satellites. Polar orbiting satellites sample only twice-per-day on ascending and descending orbits. To overcome this problem, the International Satellite Cloud Climatology Project (ISCCP) [Rossow and Schiffer, 1999] combined data available from geostationary and polar orbiting satellites. Wylie [2008] gives a summary of the diurnal variability of clouds for different regions as observed from a mixture of geostationary and polar orbiting satellites and from the observations from the ISCCP data set [Rossow and Schiffer, 1999].

[10] The MODIS Cloud Product combines infrared and visible techniques to determine both physical and radiative cloud properties. Cloud fraction, cloud top temperature, cloud top height, cloud effective emissivity, and phase (ice versus water, opaque versus nonopaque) products are produced by infrared retrieval methods for both day and night using  $5 \times 5$  bins of 1 km resolution pixels [Ackerman et al., 2006]. MODIS Collection 5 has  $1^\circ \times 1^\circ$  monthly mean cloud fractions for daytime scenes that are used in this study

(MOD08\_M3.005 and MYD08\_M3.051 for Terra and Aqua, respectively) [Frey et al., 2008; Ackerman et al., 2008, 2006]. Terra/MODIS has an equator crossing time of around 1030 local time and Aqua/MODIS is a part of the A-train with a 1330 equator crossing time. The difference in measured cloud fraction between the Terra/MODIS and Aqua/MODIS can be calculated, although the local overpass time difference between the two MODIS instruments is only 3 h and is, therefore, unable to view the entire diurnal variation. Figure 2 shows a 7 year averaged (July 2002 to July 2009) global cloud fraction difference between Terra/MODIS and Aqua/MODIS. It is evident that the afternoon orbiter (Aqua/MODIS) sees more clouds than the morning orbiter (Terra/MODIS) over land. On the other hand, Terra/MODIS shows more clouds over oceans in the morning than Aqua/MODIS shows in the afternoon, particularly over the west coasts of South America, South Africa and Australia. The large difference over Greenland and the Tibetan Plateau might be related to the cloud retrieval algorithm limitations over bright snow/ice.

[11] Figure 3 shows the monthly averaged MODIS cloud fraction time series of both Aqua and Terra for 2005–2009. As was shown in Figure 2, there are more clouds over land in the afternoon than in the morning and the opposite is true over oceans.

[12] Figure 4 shows the measured 340 nm LER time series for NOAA 18 SBUV (blue), which has a similar equator crossing time as Aqua ( $\sim 1330$  LT) and NOAA 17 (black) which has a similar time to Terra ( $\sim 1030$  LT). These are daily values smoothed with a 31 point running average. The sea and land values are plotted with a 5 RU offset (plus and minus, respectively) for visual clarity. The graphs show qualitative agreement between the data from the two different satellite platforms indicating that the MODIS measured cloud fraction and the SBUV 340 nm LER are measuring the same change in cloud cover. Both the seasonal and diurnal signals are consistent between data sets. Since the NOAA SBUV series of instruments are onboard satellites with slowly precessing orbits (see Table 1 and Figure 5) they allow us to study the diurnal LER cycle from approximately 0600 to 1800 local time.

## 3. Satellite LER Data at 340 nm

[13] A 30 year data record (1979–2008) of NUV LER satellite observations is derived using the NASA TOMS and SBUV instruments (see Table 1). Meteor 3 TOMS observations are omitted from this analysis because of the rapidly precessing orbit of the spacecraft and ongoing calibration issues; ADEOS TOMS data are excluded because of the short lifetime of the spacecraft (11 months); EarthProbe TOMS (EP) data are not used because of in-flight calibration issues affecting single wavelength measurements and the lack of a 340 nm channel. All of the remaining instrument data sets have been processed with a common retrieval algorithm based on the equations given by Herman et al. [2009], Herman [2010], and Flynn [2007].

[14] The precessing orbits of the NOAA SBUV/2 satellites (Figure 5), when combined with the overlapping near-noon orbits of the NASA satellites, provide the opportunity to measure the mean zonal average behavior of 340 nm LER throughout a daylight cycle over land and oceans.



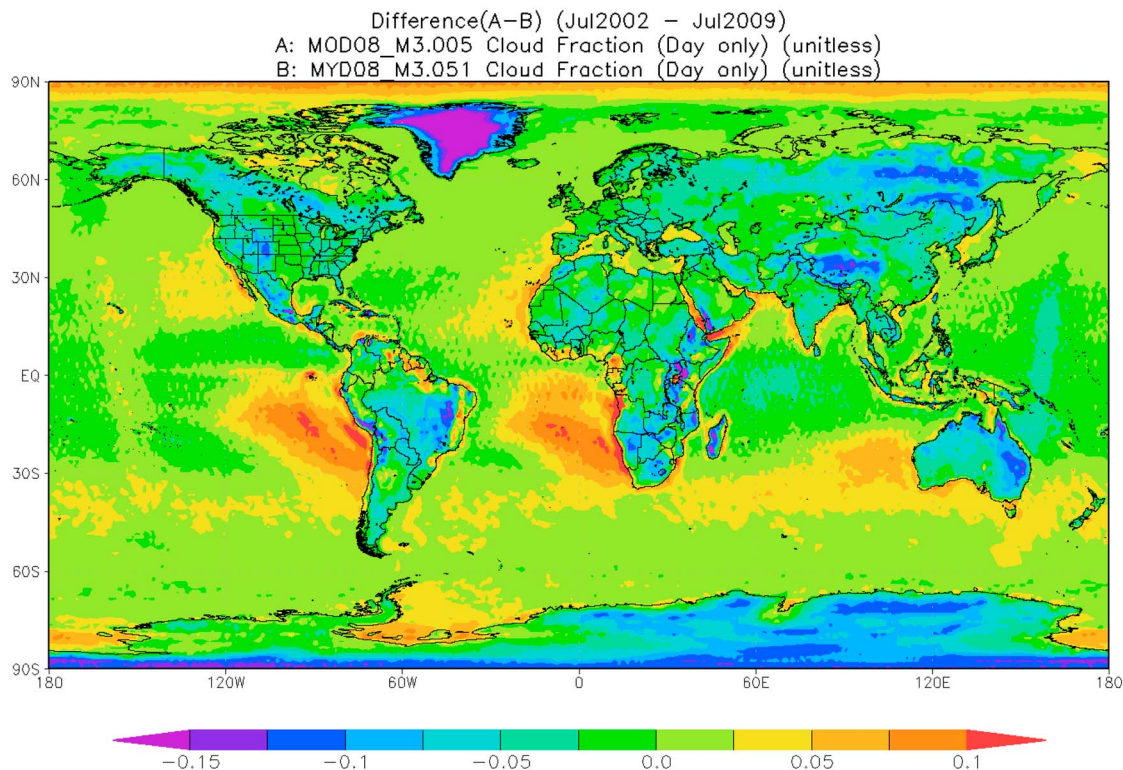


**Figure 2.** Difference in cloud fraction between 1030 and 1330 local time as measured by Terra and Aqua MODIS instruments.

The LER data used in this study are from three types of satellite instruments. The nadir viewing SBUV series of spectrometers are used which have central wavelengths from 339.75 nm to 340.05 nm with a band pass of 1.1 nm FWHM with a  $180 \times 180 \text{ km}^2$  FOV at the surface [Frederick *et al.*, 1986].

[15] Because these instruments view only in the nadir with a small FOV, it takes about two weeks to provide full global coverage. The NIMBUS 7 TOMS instrument is used which measures radiances by cross-track scanning, with a native resolution of approximately  $50 \times 50 \text{ km}^2$  at nadir, expanding to about  $100 \times 200 \text{ km}^2$  at the extreme off-nadir scan

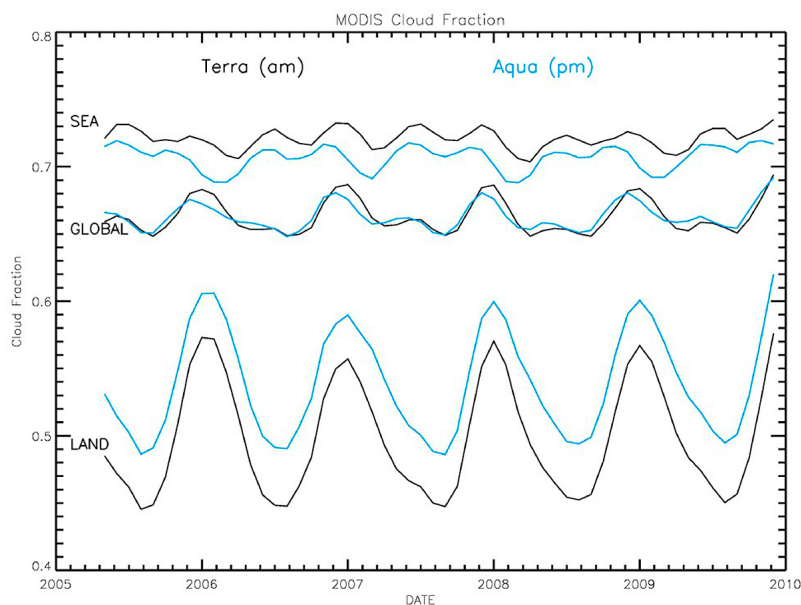


**Figure 3.** Difference in monthly mean cloud fraction between 1030 and 1330 local time as measured by MODIS on the Terra and Aqua satellites.

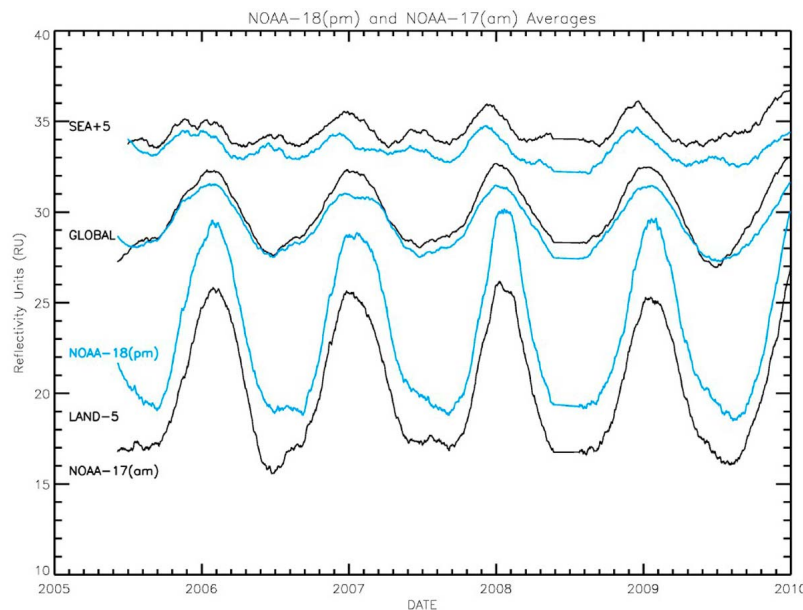


**Figure 4.** Difference LER corresponding to cloud change between 1030 and 1330 local time as measured by NOAA 17 and NOAA 18 SBUV/2 instruments. NOAA 17 is in a 1030 orbit and NOAA 18 is at 1330 local time, very similar to Terra and Aqua. The ocean and land values have a  $\pm 5$  RU offset for visual clarity.

positions ( $53^\circ$  from nadir) with daily global coverage at 340 with 0.55 FWHM nm [Heath *et al.*, 1975]. SeaWiFS (one channel at  $\lambda = 412$  with 10 nm FWHM) and OMI (1500 channels on two focal planes spanning 270–380 nm and 350–500 nm with 0.45 and 0.63 nm FWHM, respectively [Laan *et al.*, 1999]), have daily global coverage with higher spatial resolution,  $4 \times 4 \text{ km}^2$  and  $13 \times 24 \text{ km}^2$ , respectively. SeaWiFS data have been adjusted to 340 nm from the native 412 nm measurements. Data used in this study were reduced to include only near-nadir FOVs to match the SBUV FOV. Data from the OMI and SeaWiFS instruments were spectrally and spatially aggregated to a common spectral and spatial resolution corresponding to the SBUV/2 instruments (1.1 nm FWHM at 340 nm and  $180 \times 180 \text{ km}^2$ , respectively), followed by temporal and

spatial aggregation into monthly  $5^\circ$  latitude zonal means. The Nimbus 7 TOMS data were first aggregated spatially by coadding adjacent pixels (forming  $3 \times 3$  sets of TOMS pixels to match the SBUV spatial resolution) without any wavelength adjustment before aggregating into monthly  $5^\circ$  zonal bands.

#### 4. Instrument Calibration

[16] The TOMS, SBUV and SBUV/2 series of instruments were calibrated in the laboratory prior to integration on a spacecraft. The prelaunch calibration procedures include measuring and defining the monochromator wavelength scale, electronic gain ratio, nonlinearity, radiance and irradiance sensitivity, solar diffuser reflectivity, and diffuser angular

**Table 1.** Satellite Instrument 340 nm Data Sets Used in This Study

Operational Time Period	Instrument Name	Coverage and Comments	Center Wavelength (nm)	FWHM (nm)
Nov 1979 to May 1993	Nimbus 7/TOMS (N7T)	Full global coverage every day (TOMS).	340.0	0.55
Nov 1979 to Sep 1990	Nimbus 7/SBUV (N7S)	Nadir-viewing only(SBUV). Near-noon orbit.	339.9	1.10
1985 to present	SBUV/2 Series (N 9, N 11, N 14, N 16 <sup>a</sup> , N 17 <sup>a</sup> , N 18 <sup>a</sup> )	Nadir viewing only. All but N 17 and N 18 have precessing orbits from 0600 to 1800 LST.	339.75–340.05	1.10
Sep 1997 to present	SeaWiFS (SW <sup>a</sup> )	Daily global coverage. The 412 nm reflectivity produced using the TOMS retrieval algorithm. Noon orbit, later moved to 1300 to join A-Train constellation of satellites.	412.0	10.0
Aug 2004 to present	Ozone Monitoring Instrument (OMI <sup>a</sup> )	Daily global coverage. 1300 orbit.	340.0	0.55

<sup>a</sup>The indicated satellite instruments are still continuing to provide data as of 2010, but only complete years of data through 2008 are considered in this paper.

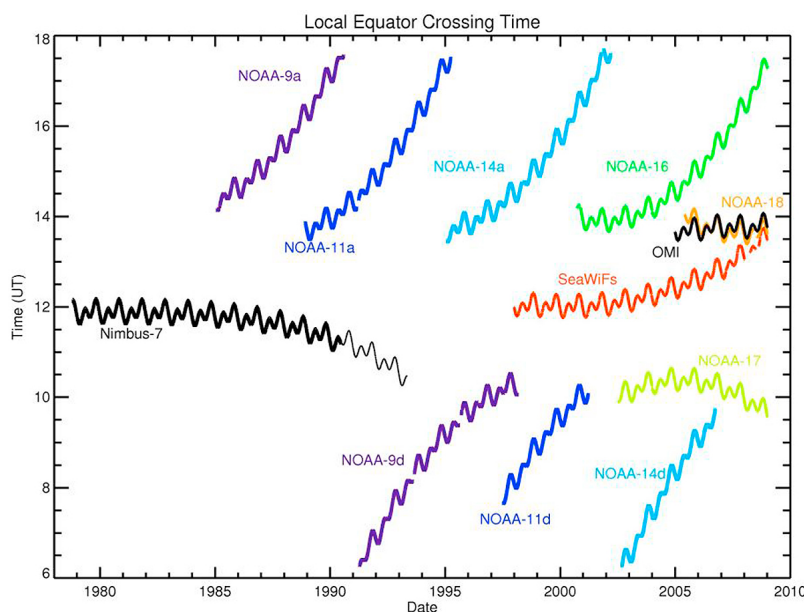


**Figure 5.** Local solar equator crossing times of the satellites indicated in Table 1.

dependence. The radiance and irradiance calibration are traceable to the National Institute of Standards and Technology (NIST) lamp radiometric standard and diffuser BRDF standards [e.g., Huang *et al.*, 1998; Janz *et al.*, 1995].

[17] The LER values reported here are derived from ratios of measured Earth radiance to measured solar irradiance by the same spacecraft instrument. These instruments measure solar irradiance by deploying a diffuser to reflect sunlight into the instrument. The SBUV/2 instruments use an onboard mercury lamp to track postlaunch changes of diffuser reflectivity. Since the solar-viewing diffuser is the only element not common to the optical path for both measurements, changes in spectrometer sensitivity should cancel out in this ratio, removing the potential impact of errors in absolute radiometric calibration. Changes in sensitivity due to both photomultiplier tube degradation and photomultiplier tube hysteresis are tracked using on-orbit data. Additional long-term calibration for the SBUV/2 instruments was provided by coincident observations with eight flights of the Shuttle SBUV (SSBUV) instrument between 1989 and 1996. In addition to simple temporal overlap of the satellite data sets, a rigorous SSBUV intercalibration campaign provided a consistent, stable calibration across the various satellite instruments [Hilsenrath *et al.*, 1995].

[18] Measurements of Antarctic and Greenland snow/ice radiances are used for cross-validation of 340 nm LER observations between instruments and for establishing long-term precision [Huang *et al.*, 2003; Jaross and Warner, 2008]. This technique assumes that the regional average snow/ice reflectivity does not change appreciably on a decadal time scale. Instrument sensitivity corrections derived from these measurements are applied to SBUV/2s after the SSBUV series of missions were terminated in 1996. On the basis of SBUV/2 snow/ice radiance and clear-sky ocean measurements, the satellite-to-satellite agreement (precision) of the LER measurements at 340 nm in the monthly zonal means is on the order of  $\pm 1$  RU [Huang *et al.*, 2003].

[19] OMI is a spectrometer with continuous wavelength coverage from 270 to 500 nm with a nominal wavelength resolution of about 0.5 nm. The OMI calibration is mainly based on its initial laboratory calibration, in-flight calibration viewing the sun reflected from a diffuser plate, and an onboard white light source. The sensitivity change at 340 nm was only  $\sim 0.5\%$  after 2.5 years of operation [Dobber *et al.*, 2008]. OMI instrumental stability has been verified using radiances measured over ice and clear-sky ocean scenes.

[20] SeaWiFS radiances have been calibrated using a comparison with underwater spectrometers (vicarious calibration) from the Marine Optical BuoY (MOBY) station near Hawaii [Eplee *et al.*, 2001], which provides the precision needed in this study. We used the 412 nm radiance data from SeaWiFS, which has a band pass of 10 nm FWHM [SeaWiFS users guide]. These radiances were adjusted to correspond to the SBUV/2 instruments' 1.1 nm FWHM at 340 nm using simultaneously measured OMI radiance data at the two wavelengths (412 and 340 nm) as the transfer standard. The difference in LER values between 412 nm and 340 nm are due to vegetation cover on land and chlorophyll and colored dissolved organic matter (CDOM) effects over the oceans. Analysis of these differences shows that there is a mean systematic difference of approximately  $2 \pm 1$  RU between the overlapping 340 nm SBUV/2 and SeaWiFS 412 nm LER measurements. For this study, a constant 2 RU has been added to all of the SeaWiFS 412 nm LER values to bring it into agreement with overlapping OMI 340 nm LER.

## 5. Zonal Average 340 nm LER

[21] When the LER data are combined into annual zonal averages for the satellite instruments listed in Table 1, the distribution of LER with latitude is shown in Figure 6, with minimum values at the equator and maximum values at high latitudes. In the Northern Hemisphere (NH), the higher values are caused by clouds over snow and ice during winter



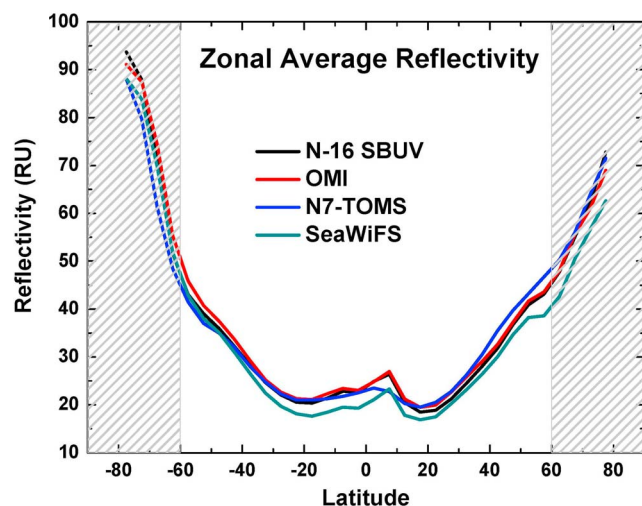


**Figure 6.** The zonal average reflectivity data from NOAA 16 SBUV/2 (2001–2008), OMI (2005–2008), N7-TOMS (1979–1992), and SeaWiFS (1998–2008).

months. However, in the Southern Hemisphere (SH), the high values between 50°S and 70°S are entirely caused by clouds over mostly ice-free oceans. The local maximum at 5°N is associated with the Intertropical Convergence Zone (ITCZ) and large El Niño events. The annual and zonal average LER data from the various satellites are in close agreement, with some indication of small secular changes and possible small differences in calibration. The global area weighted average LER for the data shown in Figure 6 is approximately 30 RU.

## 6. Estimating LER Diurnal Variability

[22] To examine the diurnal behavior of LER over land and oceans, data from satellites with non-noon orbits were

compared with those having near-noon orbits (see Figure 5). Each individual LER measurement is time-stamped with its local solar time (LST). The data taken from each satellite were placed into 5° zonal means calculated for land and oceans separately. Data were then placed into 5 min LST average bins, smoothed with an 11 point running average (~1 h average), and plotted as a function of LST as shown in Figures 7 through 10.

[23] Figure 7 shows a near-noon LER minimum for both land and oceans in the 12.5°S latitude band, but with a much stronger afternoon increase in LER over land compared to the oceans, where the afternoon increase in LER relative to noon is smaller than the morning values. The behavior in the 27.5°N band is different (Figure 8). Here the daily minimum occurs closer to 1100 LST with almost no change between the morning LER and 1100 LST. There is an increase in LER between 1100 and 1300 LST, which then remains fairly constant throughout the afternoon. This is in contrast to the ocean behavior, where the higher morning LER decreases until 1100 LST and then increases until 1600 LST.

[24] Meteorological observations are consistent with these findings, and show that over water at low latitudes there is a persistent boundary layer of mist and fog in the morning because of high relative humidity from low air temperatures and high dew point temperatures from ocean spray [Bergman and Salby, 1996]. Toward noon, as the air temperature rises, the low-level mist and fog decreases as the relative humidity decreases, resulting in the lower reflectivity values. In the late afternoon and evening, as the air temperatures continue to rise, afternoon convection leading to widespread cumulus and cumulonimbus cloud production results in the higher reflectivity values. A similar effect can be seen in the land measurements because of high early morning dew points over predominantly jungle vegetation, particularly over the Amazon region of South America [Kondragunta and Gruber, 1994]. A similar clearing effect to that over the water is seen toward noon as the air temperature rises. In the late

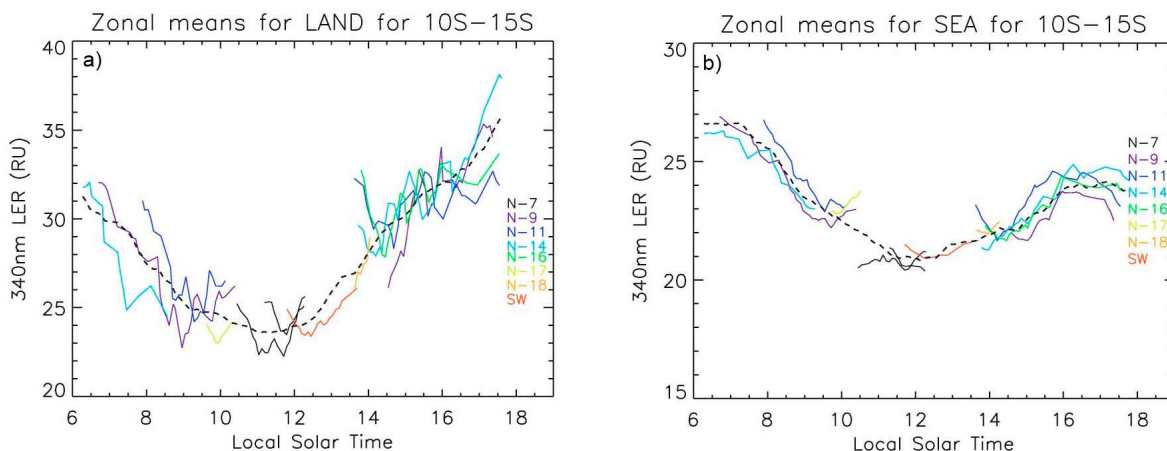


**Figure 7.** Changes in LER as a function of time-of-day for (a) land and (b) ocean from ~0600 to 1800 local time for a 5° latitude band from 10 to 15°S. The specific orbits of the NOAA series of satellites never passed through a noontime orbit, thus limiting their measurements to approximately 0600–1030 and 1330–1800 local time. The noontime measurements were made by Nimbus 7 TOMS and SBUV (black lines) as well as SeaWiFS (red line).



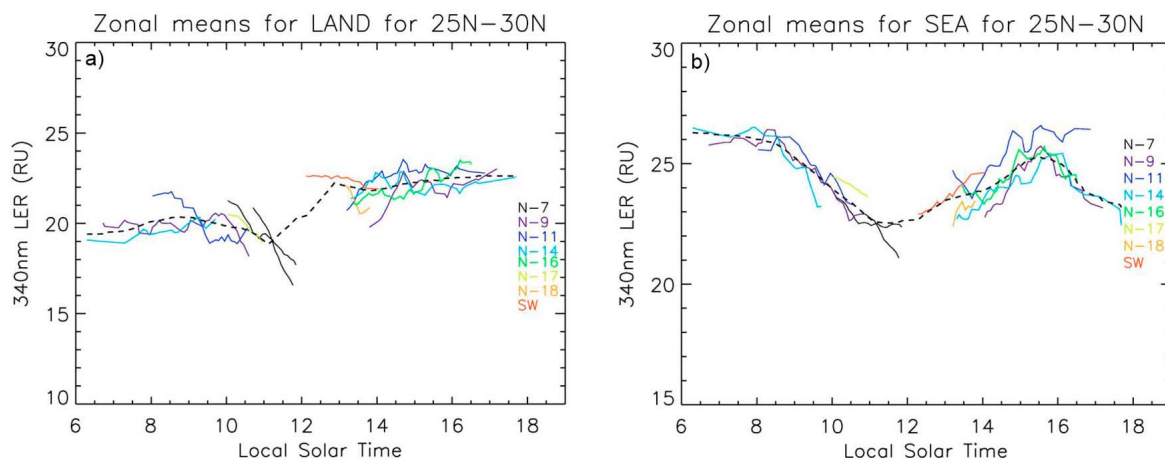


**Figure 8.** Similar to Figure 7 but for 25–30°N.

afternoon significantly more cumulus convection occurs over land than over the oceans. At the middle northern latitudes over land, the air tends to be dry and the reflectivities in the morning and toward noon tend to be low with generally clearer skies and lower dew points consistent as shown in Figure 8. Toward late afternoon and evening, as the land heats up and air temperatures rise, cumulus convection produces more clouds [Cairns, 1995], which result in the higher reflectivity values seen over land. Over water, the reflectivity pattern is a result of similar circumstances to that seen in the low southern latitudes: high dew points from ocean spray and low air temperatures in the morning producing high reflectivities, clearing toward noon as the air temperatures rise producing lower reflectivities, and cumulus production in the late afternoon and evening resulting in higher reflectivity values [Bergman and Salby, 1996].

[25] The smoothed averaged data for the 5° latitude bands over oceans from 60°S–60°N are shown in Figures 9a and 9b. The general shape of the diurnal variation of ocean LER is

similar as a function of latitude with increasing values toward higher latitudes in both hemispheres corresponding to the increased amount of cloud cover. Both hemispheres exhibit almost the same increase in mean zonal cloud amount with the exception of the northern tropics (equator to 10°N) which shows more cloud cover than the southern tropics, particularly in the afternoon. The absolute change between morning and noontime LER is on the order of 2–4 RU, but the relative change (in percent) can be significantly more in the tropics (10–20%) than at midlatitudes (~5%). The LER values of several latitude bands at seven select times throughout the day for both land and oceans are presented in Table 2.

[26] Figures 10a–10c show the diurnal variation of LER over landmasses. As was shown previously, the afternoon values are generally greater than the morning consistent with cloud formation caused by convective heating. However, the tropics and the region from 10°N–20°S exhibit a markedly different pattern where there is a more symmetric

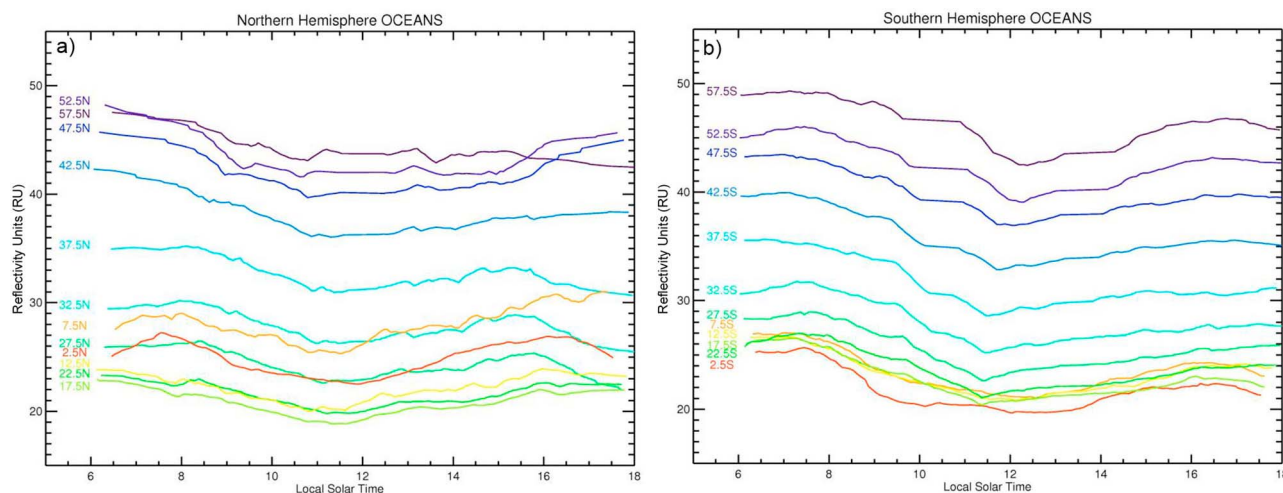


**Figure 9.** (a) The smoothed averaged zonal mean values for the Northern Hemisphere oceans for each 5° latitude band from the equator to 60°N. (b) Same as Figure 9a but for Southern Hemisphere.

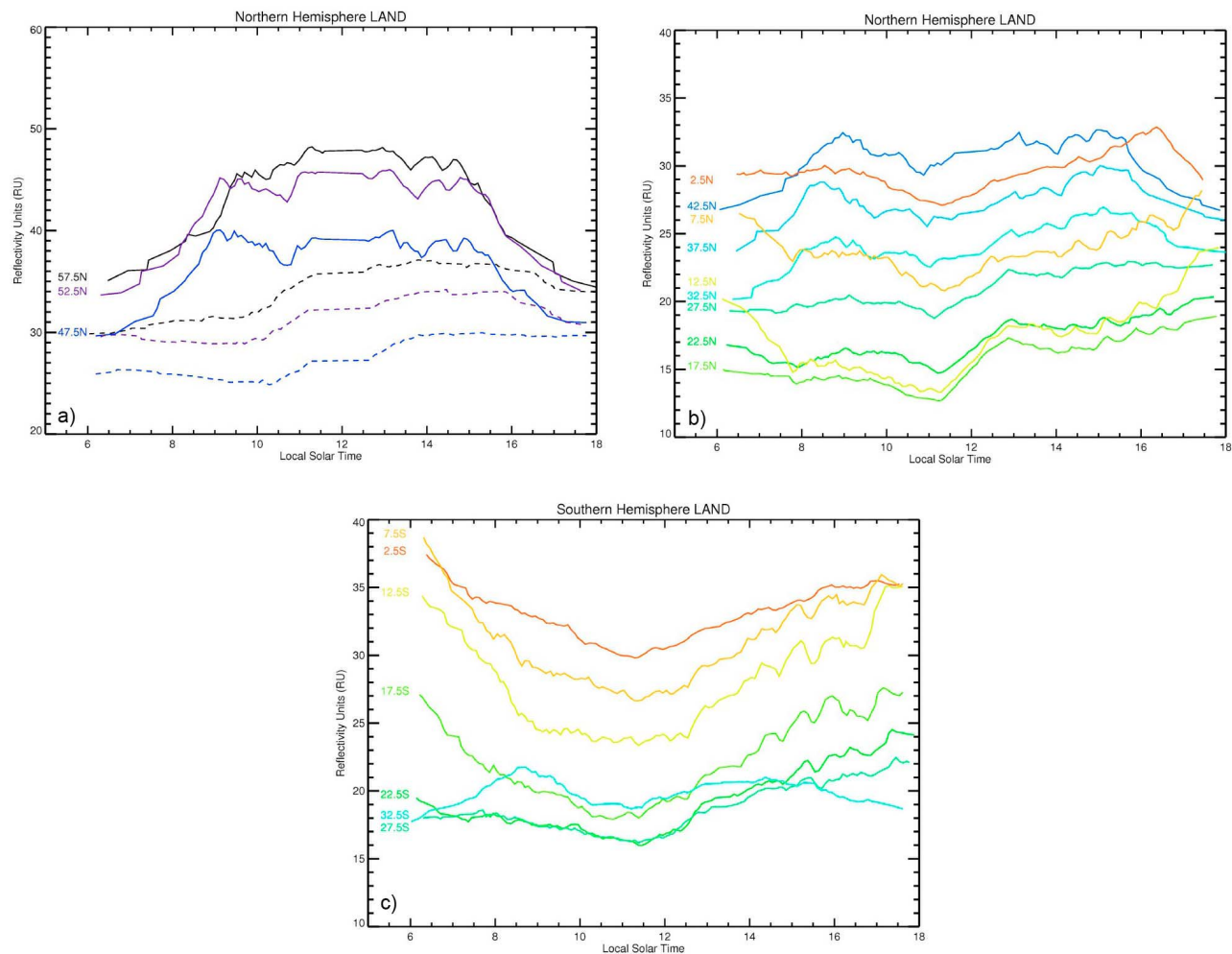


**Figure 10.** (a) The smoothed averaged zonal mean values for the Northern Hemisphere land for each 5° band from 45°N to 60°N. The solid line is an annual average and the dashed line is summer only (May–August). (b) The smoothed averaged zonal mean values for the Northern Hemisphere land for each 5° band from the equator to 45°N. (c) Same as Figure 9a but for Southern Hemisphere over land. The latitude range is limited by insufficient amount of land area between 30°S and 60°S to form zonal average LER.

shape, with the morning having equal or greater cloud amount than the afternoon. This is due to high early morning humidity in the southern hemisphere monsoon regions, such as the Congo and Amazon River basins from the jungle vegetation. As the air warms through the morning and afternoon, the relative humidity and clouds decrease. Also, there is a persistent early morning stratocumulus cloud layer off of the South American coast in the southeast Pacific which gets dissipated as the day wears on [Kondragunta and Gruber, 1994]. Southward of 20°S, the pattern reverts back to the shape seen in the northern hemisphere. Northward of 45°N, a large diurnal signal is due to snow/ice on the ground during the winter season. The dashed lines represent non-winter months of May–August. Because the satellite NUV measurements have no way of discriminating between snow/ice and clouds, there is no method available to calculate a true annual average for the highest three latitude bands in the northern hemisphere. There is not enough land south of

35°S to create a reasonable representative zonal mean. An alternative way to plot the zonal mean LER cloud amount is as a function of fractional daylight (heating) from sunrise to sunset. These curves are shown in Figures 11a–11d. The curves are quite similar to those shown in Figure 10, with some slight differences in the early morning and late afternoon. This decrease in LER is most likely due to shadowing of the clouds at very high solar zenith angles.

## 7. Summary

[27] Thirty years of satellite measurements of 340 nm Lambert equivalent reflectivity (LER) have been analyzed to show the changes in diurnal LER that are associated with cloud and aerosol amounts. The diurnal variation of LER is obtained from multiple NASA and NOAA satellites making 340 nm LER measurements at 5 degree zonal means as a function of time of day as well as fraction of day (daylight

**Table 2.** Numerical Values for Seven Selected Times Throughout the Day for Land and Ocean<sup>a</sup>

Latitude Band	Average LER 0730	Average LER 0900	Average LER 1030	Average LER 1200	Average LER 1330	Average LER 1500	Average LER 1630
<i>Over Land</i>							
55–60°N	37.1	41.9	46.0	47.8	47.0	45.4	38.3
50–55°N	35.8	43.5	43.8	45.6	44.5	44.2	37.9
45–50°N	32.1	38.8	37.7	39.1	38.7	38.3	33.1
40–45°N	28.8	31.9	30.2	31.0	31.7	32.3	29.0
35–40°N	26.2	27.8	26.5	26.6	28.0	29.7	27.8
30–35°N	22.3	24.3	23.3	23.5	25.3	26.5	25.2
25–30°N	19.5	20.1	19.7	20.4	22.0	22.6	22.7
20–25°N	15.5	16.2	15.8	16.4	18.3	18.3	19.2
15–20°N	14.4	14.3	13.2	15.0	16.7	16.8	17.9
10–15°N	16.2	15.2	13.8	15.6	18.1	18.1	20.2
5–10°N	24.0	23.5	22.0	22.0	23.5	24.4	25.9
Equator–5°N	29.4	29.6	27.9	27.9	29.7	30.8	32.1
5°S–Equator	34.3	32.7	30.6	30.6	32.5	33.8	35.1
5–10°S	32.5	29.1	27.7	27.3	30.0	32.8	34.0
10–15°S	30.1	24.8	23.8	24.0	27.1	29.8	31.1
15–20°S	22.4	20.1	18.2	19.2	21.8	24.8	25.9
20–25°S	18.1	17.6	16.7	16.8	19.7	21.2	22.8
25–30°S	18.3	17.5	16.7	16.8	19.0	20.5	21.1
30–35°S	19.8	21.3	19.1	19.5	20.6	20.6	19.4
<i>Over Ocean</i>							
55–60°N	47.0	45.0	43.4	43.7	43.5	43.9	43.1
50–55°N	47.0	43.5	42.0	42.0	42.1	42.2	44.9
45–50°N	45.0	42.3	40.4	40.1	40.6	41.1	43.5
40–45°N	41.1	39.2	36.9	36.3	36.9	37.7	38.0
35–40°N	35.0	34.2	31.9	31.2	32.0	33.1	31.7
30–35°N	29.9	29.3	27.2	26.5	27.2	28.6	27.3
25–30°N	26.1	25.5	23.5	23.0	23.7	24.8	24.2
20–25°N	22.6	22.1	20.6	20.1	20.9	21.5	22.5
15–20°N	21.9	21.0	19.4	19.3	20.3	20.9	21.7
10–15°N	23.0	21.9	20.4	20.8	21.9	22.6	23.6
5–10°N	28.7	27.5	26.1	26.3	27.8	29.0	30.4
Equator–5°N	26.8	24.8	23.3	22.7	24.4	26.1	26.7
5°S–Equator	25.3	21.9	20.4	19.9	20.2	21.8	22.2
5–10°S	26.6	23.9	22.1	21.2	21.8	23.3	24.2
10–15°S	26.1	23.6	22.0	20.9	21.7	22.5	23.9
15–20°S	26.2	23.9	21.8	20.8	21.4	21.8	22.8
20–25°S	26.9	25.1	22.9	21.6	22.1	22.8	23.8
25–30°S	28.8	27.1	24.5	23.3	24.1	24.7	25.5
30–35°S	31.5	30.0	27.1	25.7	26.5	27.1	27.6
35–40°S	35.2	33.9	30.6	29.0	30.0	30.7	30.6
40–45°S	39.6	37.7	34.9	33.1	33.8	34.8	35.5
45–50°S	43.1	41.3	39.2	37.1	37.9	38.8	39.6
50–55°S	45.8	44.1	42.1	39.6	40.1	41.7	43.0
55–60°S	49.2	48.0	46.4	43.0	43.3	45.3	46.6

<sup>a</sup>The values are calculated from the 340 nm LER measurements that are within  $\pm 30$  min of the displayed time. There is not enough land south of 35° to make statistically significant zonal mean. Northward from 5°N, the ocean values are higher than their land counterparts, whereas from 20°S–5°N the opposite is true.

only). These zonal means were calculated separately over water and land. The results show different behavior of clouds over oceans with LER peaking in the morning compared to LER over land, which peaks in the afternoon. Over the oceans the cloud amount increases as a function of latitude in both hemispheres, with the exception of the midtropics (10–20°). Over land, the amount of cloudiness significantly decreases by almost a factor of 2 from the Equator to  $\sim 25^\circ$  and then, in the northern hemisphere, increases as a function of latitude. Measurements of cloud fraction made by Aqua and Terra MODIS show a signature that is similar to LER in morning to afternoon cloud fraction ratios. The similarity in pattern demonstrates that the LER is measuring a quantity directly related to cloud fraction. The similarity in pattern between LER and cloud fraction demonstrates that the energy

reflected back to space depends more on cloud fraction than it does on cloud optical depth. This is because the amount of light reflected from clouds is nearly insensitive to cloud optical depth changes for clouds with large optical depths. The use of LER in place of cloud fraction removes the need to consider subpixel cloud fractions or very high spatial resolution for cloud fraction, to estimate the energy reflected back to space.

## Appendix A

[28] Lambert equivalent reflectivity: The Lambert equivalent reflectivity  $R$  represents the equivalent scene reflectivity (the combined effect of the surface  $R_G$ , clouds, water haze, and aerosols) after removal of Rayleigh scattering effects.  $R$

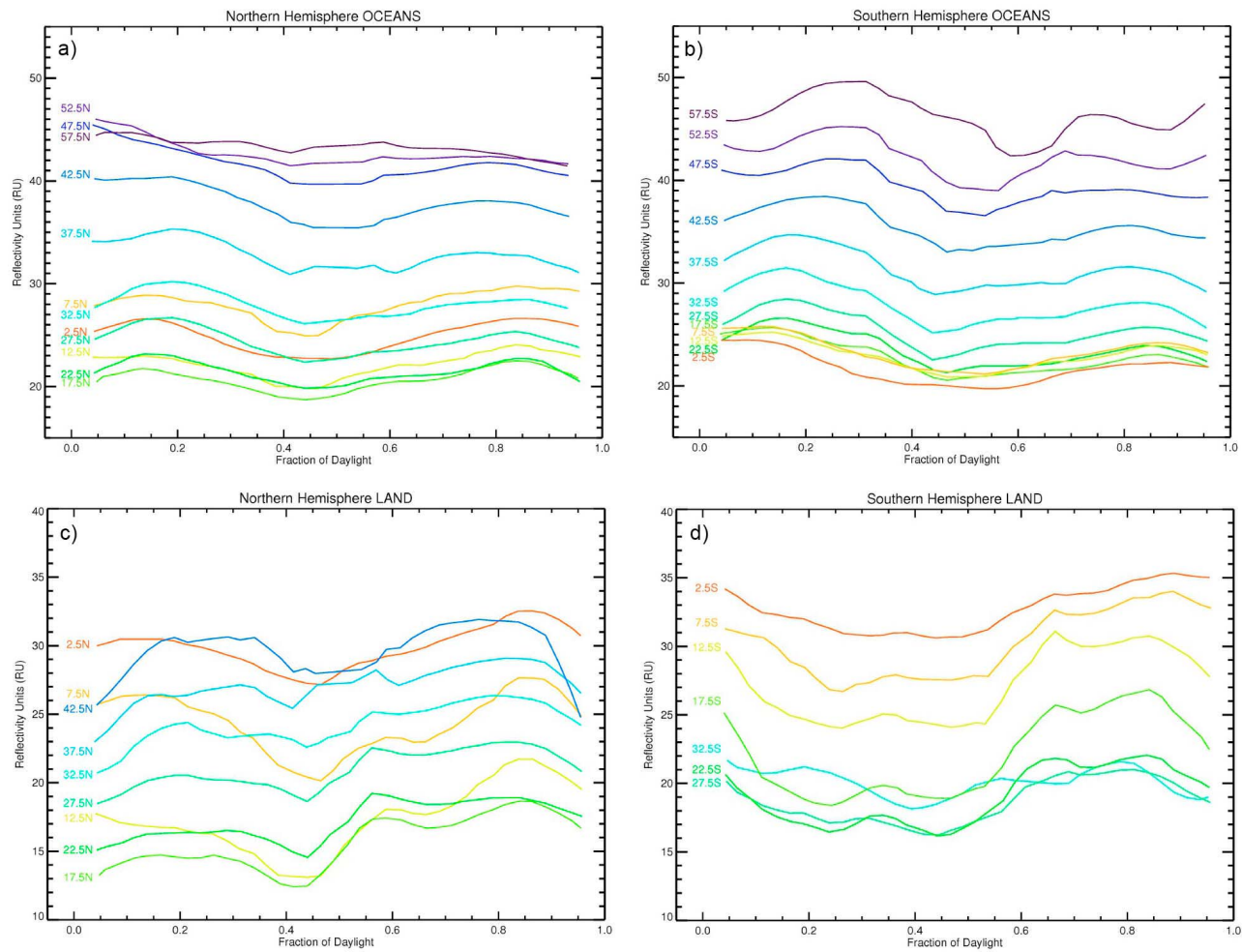


**Figure 11.** (a) Northern and (b) Southern Hemisphere oceans plotted as a function of fraction of daylight. (c) Northern and (d) Southern Hemisphere land plotted as a function of fraction of daylight.

is an approximation to the angular average reflectivity, since it is based on only a small subset of the Earth's BRDF (bidirectional reflectivity distribution function).

[29]  $R$  is calculated by requiring that the measured radiance  $I_{SM}$  match the calculated radiance  $I_S$  at the observing position of the satellite (equation (A1)) by adjusting a single free parameter  $R$  in the formal solution of the radiative transfer equation

$$I_S(\Omega, \Theta, R, P_O) = \frac{RI_d(\Omega, \Theta, P_O)f(\Omega, \Theta, P_O)}{1 - RS_b(\Omega, P_O)} + I_{dO}(\Omega, \Theta, P_O) = I_{SM} \quad (A1)$$

where

- $\Omega$  ozone amount from shorter wavelengths (e.g., 300–330 nm);
- $\Theta$  viewing geometry (solar zenith angle, satellite look angle, azimuth angle);
- $P_O$  pressure of the reflecting surface assumed at the local ground altitude;
- $R$  LER at  $P_O$ ;
- $S_b$  fraction scattered back to  $P_O$  from the atmosphere;
- $I_d$  sum of direct and diffuse irradiance reaching  $P_O$ ;

$f$  fraction of radiation reflected from  $P_O$  reaching the satellite;

$I_{dO}$  radiance scattered back from the atmosphere for  $R = 0$  and  $P = P_O$ .

[30] The quantities  $S_b$ ,  $I_d$ ,  $F$ , and  $I_{dO}$  are calculated from radiative transfer solutions for atmospheres similar to the measured case.

[31] Rearranging equation (A1) gives the LER values  $R$  (equation (A2))

$$R = \frac{I_{SM} - I_{dO}}{I_d f + (I_{SM} - I_{dO})S_b}. \quad (A2)$$

[32] **Acknowledgments.** We would like to thank the NASA Ozone Processing Team for providing level 2 data from the NASA and NOAA satellites, NASA headquarters' Making Earth System data records for Use in Research EnvironmentS (MEASURES) program for funding this work. The LER data is publically available at <ftp://toms.gsfc.nasa.gov/pub/tmp/herman/measures>. The MODIS cloud fraction figures were produced with the Giovanni online data system, developed and maintained by the NASA GES DISC. We also acknowledge the MODIS mission scientists and associated NASA personnel for the production of the cloud fraction data used in this study. Also, we would like to thank David Haffner for providing OMI operational retrieval code and Albert Huang for processing OMI LER.



## References

- Ackerman, S., K. Strabala, P. Menzel, R. Frey, C. Moeller, L. Gumley, B. Baum, S. W. Seemann, and H. Zhang (2006), Discriminating Clear-Sky From Cloud With MODIS Algorithm Theoretical Basis Document (MOD35), Version 5.0, Coop. Inst. for Meteorol. Satell. Stud., Univ. of Wis., Madison.
- Ackerman, S. A., R. E. Holz, R. Frey, E. W. Eloranta, B. C. Maddux, and M. McGill (2008), Cloud detection with MODIS. Part II: Validation, *J. Atmos. Oceanic Technol.*, 25(7), 1073–1086, doi:10.1175/2007JTECHA1053.1.
- Bergman, J. W., and M. L. Salby (1996), Diurnal variations of cloud cover and their relationship to climatological conditions, *J. Clim.*, 9(11), 2802–2820, doi:10.1175/1520-0442(1996)009<2802:DVOCCA>2.0.CO;2.
- Boersma, K. F., H. J. Eskes, and E. J. Brinksma (2004), Error analysis for tropospheric NO<sub>2</sub> retrieval from space, *J. Geophys. Res.*, 109, D04311, doi:10.1029/2003JD003962.
- Cairns, B. (1995), Diurnal variations of cloud from ISCCP data, *Atmos. Res.*, 37(1–3), 133–146, doi:10.1016/0169-8095(94)00074-N.
- Chandrasekhar, S. (1960), *Radiative Transfer*, Dover, Mineola, N. Y.
- Chen, S. S., and R. A. Houze (1997), Diurnal variation and life-cycle of deep convective systems over the tropical Pacific warm pool, *Q. J. R. Meteorol. Soc.*, 123, 357–388, doi:10.1002/qj.49712353806.
- Dave, J. V. (1964), Meaning of successive iteration of the auxiliary equation in the theory of radiative transfer, *Astrophys. J.*, 140, 1292–1303, doi:10.1086/148024.
- Dave, J. V., and P. Furukawa (1964), The effect of Lambert-type ground reflection on Umkehr measurements, *J. Atmos. Sci.*, 21(2), 161–167, doi:10.1175/1520-0469(1964)021<0161:TEOLTG>2.0.CO;2.
- Dobber, M., Q. Kleipool, R. Dirksen, P. Levelt, G. Jaross, S. Taylor, T. Kelly, L. Flynn, G. Leppelmeier, and N. Rozemeijer (2008), Validation of Ozone Monitoring Instrument level 1b data products, *J. Geophys. Res.*, 113, D15S06, doi:10.1029/2007JD008665.
- Eplee, R. E., Jr., W. D. Robinson, S. W. Bailey, D. K. Clark, P. J. Werdell, M. Wang, R. A. Barnes, and C. R. McClain (2001), Calibration of SeaWiFS. II. Vicarious techniques, *Appl. Opt.*, 40(36), 6701–6718, doi:10.1364/AO.40.006701.
- Flynn, L. (2007), Solar Backscatter Ultraviolet Instrument (SBUV/2) Version 8 Ozone Retrieval Algorithm Basis Document, V8 ATBD, NOAA Natl. Environ. Satell., Data and Inf. Serv., Camp Springs, Md.
- Frederick, J. E., R. P. Cebula, and D. F. Heath (1986), Instrument characterization for the detection of long-term changes in stratospheric ozone: An analysis of the SBUV/2 radiometer, *J. Atmos. Oceanic Technol.*, 3, 472–480, doi:10.1175/1520-0426(1986)003<0472:ICFTDO>2.0.CO;2.
- Frey, R. A., S. A. Ackerman, Y. Liu, K. I. Strabala, H. Zhang, J. R. Key, and X. Wang (2008), Cloud detection with MODIS. I: Improvements in the MODIS cloud mask for collection 5, *J. Atmos. Oceanic Technol.*, 25, 1057–1072, doi:10.1175/2008JTECHA1052.1.
- Heath, D. F., A. J. Krueger, H. A. Roeder, and B. D. Henderson (1975), The Solar Backscatter Ultraviolet and Total Ozone Mapping Spectrometer (SBUV/TOMS) for Nimbus G, *Opt. Eng.*, 14, 323–331.
- Herman, J. R. (2010), Global increase in UV irradiance during the past 30 years (1979–2008) estimated from satellite data, *J. Geophys. Res.*, 115, D04203, doi:10.1029/2009JD012219.
- Herman, J. R., and E. A. Celarier (1997), Earth surface reflectivity climatology at 340 nm to 380 nm from TOMS data, *J. Geophys. Res.*, 102(D23), 28,003–28,011, doi:10.1029/97JD02074.
- Herman, J. R., G. Labow, N. C. Hsu, and D. Larko (2009), Changes in cloud cover (1998–2006) derived from reflectivity time series using SeaWiFS, N7-TOMS, EP-TOMS, SBUV-2, and OMI radiance data, *J. Geophys. Res.*, 114, D01201, doi:10.1029/2007JD009508.
- Hilsenrath, E., R. P. Cebula, M. T. DeLand, K. Laamann, S. Taylor, C. Wellemeyer, and P. K. Bhartia (1995), Calibration of the NOAA-11 Solar Backscatter Ultraviolet (SBUV/2) ozone data set from 1989 to 1993 using in-flight calibration data and SSBUV, *J. Geophys. Res.*, 100(D1), 1351–1366, doi:10.1029/94JD02611.
- Huang, L. K., R. P. Cebula, and E. Hilsenrath (1998), New procedure for interpolating NIST FEL lamp irradiances, *Metrologia*, 35(4), 381–386, doi:10.1088/0026-1394/35/4/27.
- Huang, L.-K., R. P. Cebula, S. L. Taylor, M. T. DeLand, R. D. McPeters, and R. S. Stolarski (2003), Determination of NOAA-11 SBUV/2 radiance sensitivity drift based on measurements of polar ice cap radiance, *Int. J. Remote Sens.*, 24(2), 305–314, doi:10.1080/014311603004978.
- Janz, S., E. Hilsenrath, J. Butler, D. F. Heath, and R. P. Cebula (1995), Uncertainties in radiance calibrations of backscatter ultraviolet (BUV) instruments, *Metrologia*, 32(6), 637–641, doi:10.1088/0026-1394/32/6/48.
- Jaross, G., and J. Warner (2008), Use of Antarctica for validating reflected solar radiation measured by satellite sensors, *J. Geophys. Res.*, 113, D16S34, doi:10.1029/2007JD008835.
- Kelly, M. A., S. A. Lloyd, and W. H. Swartz (2006), Comparison of a 27-yr composite TOMS/SBUV(2)/OMI data set of UV Lambertian equivalent reflectivity with the shortwave albedo from ERBE and CERES, *Eos Trans. AGU*, 87(52), Fall Meet. Suppl., Abstract A23B-0950.
- Koelemeijer, R. B. A., J. F. de Haan, J. W. Hovenier, and P. Stammes (2003), A database of spectral surface reflectivity in the range 335–772 nm derived from 5.5 years of GOME observations, *J. Geophys. Res.*, 108(D2), 4070, doi:10.1029/2002JD002429.
- Kondragunta, C. R., and A. Gruber (1994), Diurnal variation of the ISCCP cloudiness, *Geophys. Res. Lett.*, 21(18), 2015–2018, doi:10.1029/94GL01459.
- Laan, E., J. de Vries, P. Levelt, P. Stammes, H. Saari, J. Lundell, A. Maelkki, and G. Leppelmeier (1999), Ozone monitoring in the next millennium with the OMI instrument, paper presented at 50th IAF Congress, Int. Astronaut. Fed., Amsterdam.
- Labow, G. J., J. R. Herman, D. Larko, L. Huang, J. Mao, and W. Qin (2009), Cloud and aerosol amounts as a function of time of day as measured by TOMS, SeaWiFS and SBUV instruments, *Eos Trans. AGU*, 90(52), Fall Meet. Suppl., Abstract A54C-07.
- Lloyd, S. A. (2005), Analysis of trends and solar cycle effects in the TOMS and SBUV(2) UV effective reflectivity data sets, *Eos Trans. AGU*, 86(52), Fall Meet. Suppl., Abstract A43C-0110.
- Lloyd, S. A. (2006a), A 27-year composite data set of global UV effective reflectivity from the TOMS and SBUV(2) satellite instruments, paper presented at 2006 Solar Radiation and Climate Experiment (SORCE) Science Meeting, Orcas Is., Wash.
- Lloyd, S. A. (2006b), Trends in Southern Hemisphere albedo using a 27-yr composite TOMS/SBUV(2)/OMI data set of UV Lambertian equivalent reflectivity, *Eos Trans. AGU*, 87(52), Fall Meet. Suppl., Abstract A32A-05.
- Lloyd, S. A., and M. DeLand (2006), A 27-year composite data set of global UV effective reflectivity from the TOMS and SBUV(2) satellite instruments, *Eos Trans. AGU*, 87(36), Jt. Assem. Suppl., Abstract A21A-03.
- Qin, W., J. R. Herman, G. R. Jaross, and G. J. Labow (2009), Global surface reflectivity study relating 340 nm SBUV narrow band LER to 412 nm SeaWiFS broadband LER using OMI spectrally resolved data, *Eos Trans. AGU*, 90(52), Fall Meet. Suppl., Abstract A13A-0193.
- Rossow, W. B., and R. A. Schiffer (1999), Advances in understanding clouds from the ISCCP, *Bull. Am. Meteorol. Soc.*, 80, 2261–2287, doi:10.1175/1520-0477(1999)080<2261:AIUCFI>2.0.CO;2.
- Wylie, D. P. (2008), Diurnal cycles of clouds and how they affect polar-orbiting satellite data, *J. Clim.*, 21(16), 3989–3996, doi:10.1175/2007JCLI2027.1.
- Wylie, D. P., and H. M. Woolf (2002), The diurnal cycle of upper tropospheric clouds measured by GOES-VAS and the ISCCP, *Mon. Weather Rev.*, 130, 171–179, doi:10.1175/1520-0493(2002)130<0171:TDCOUT>2.0.CO;2.

M. T. DeLand, L.-K. Huang, G. J. Labow, D. E. Larko, and W. Qin, Science Systems and Applications, Inc., Lanham, MD 20706, USA. (labow@lglass.gsfc.nasa.gov)

J. R. Herman, Joint Center for Earth Systems Technology Center, University of Maryland Baltimore County, Catonsville, MD 21228, USA. S. A. Lloyd, Wyle Information Services, McLean, VA 22102, USA.

J. Mao, Goddard Earth Sciences and Technology Center, University of Maryland Baltimore County, Catonsville, MD 21228, USA.